Electrically tunable graded index planar lens based on graphene

H. Nasari[a] and M. S. Abrishamian
Department of Electrical and Computer Engineering, K. N. Toosi University of Technology, Tehran 16314, Iran

(Received 13 May 2014; accepted 16 August 2014; published online 27 August 2014)

The realization of electrically tunable beam focusing using a properly designed conductivity pattern along a strip on a background single graphene flake with operation in the terahertz regime is proposed and numerically investigated. The strip is illuminated with a guided surface plasmon polaritons (SPP) plane wave and the physical origin of the design procedure is evaluated from the phase of effective mode index of propagating SPP wave on graphene. Upon tuning a gate voltage between the graphene sheet and the substrate, the focus tuning is achieved. Finite- difference time-domain numerical technique is employed to explore the propagation characteristic of SPP wave and the performance parameters of the lens include the focal length, full-width half-maximum, and focusing efficiency. Such a one atom thick planar lens with the capability of electrical focus tuning besides the compatibility with current planar optoelectronic systems can find valuable potential applications in the field of transformational plasmon optics. © *2014 AIP Publishing LLC*.
[http://dx.doi.org/10.1063/1.4894140]

I. INTRODUCTION

In the recent years, we have witnessed a rapidly growing interest in the terahertz technology for communication, imaging, and spectroscopic applications. Unfortunately, the lack of standard natural materials in the terahertz gap region of the electromagnetic spectrum that properly responds to the terahertz radiation has obstructed the effective manipulation of light in these frequencies. Although metamaterials approach can be considered as a solution, the complexity in fabrication process remains as a dilemma.[1] Graphene, an atomically thin crystalline sheet of carbon atoms organized in a honeycomb lattice, has been suggested as a possible material that may remedy these limitations after its first isolation in 2004. Owing to its unique band structure characterized by conical valence and conduction bands joined by just two Dirac points at the Fermi level, exceptional physical and optical phenomena have been revealed, which makes it a promising candidate as a versatile optical material for realization of a new generation of optical devices.[2–4] The optical conductance of graphene based devices has placed it at the center of significant research effort driven by telecommunication purposes in the infrared regime as well as ubiquitous new applications in the terahertz gap region of the electromagnetic spectrum such as security technology, quality control in the pharmaceutics industry, astronomy, and sensing.[5] A variety of optical devices on the basis of the tunable optical conductivity of graphene are numerically and/or experimentally investigated such as: graphene plasmonic cloak,[6] photo detectors,[7] modulators,[8] switches,[9] filters,[10] sensors,[11] polarizers,[12] and so on. In addition to the aptitude of optical conductance of graphene to be controlled via external electric or magnetic field, more confinement and longer propagation length besides the supporting of both transverse electric (TE) and transverse magnetic (TM) surface plasmons on the boundary of graphene and dielectric, make it as a more appropriate option in comparison with noble metals in surface plasmon polariton (SPP) based devices.[13] The presence of well-known techniques to fabricate graphene, such as mechanical exfoliation,[2] reduction of chemically exfoliated graphene oxide,[14] thermal decomposition of silicon carbide,[15] and chemical vapor deposition (CVD)[16] makes our interesting dreams about graphene based meta devices feasible. It is worthy of note that the thickness and purity of the produced graphene layer can also be determined by some techniques such as Raman spectroscopy[17] and atomic force microscopy (AFM).[18]

Tunable beam focusing is one of the most important concepts in optics, which is commonly involved in a variety of optical components and applications such as optical data processing, imaging and concentrating of light. Certainly, the rapid focus tuning on relatively small platforms cannot be achieved by mechanical approaches. One of the most promising nonmechanical approaches is the electrical one, which has the merits of easy implementation and fast response time. In this contribution, we propose graphene as a platform to achieve electrical focus tuning in the terahertz gap frequencies, based on the electrical tunability of graphene conductivity, which has some superiorities in comparison with its dielectric and noble metal based plasmonic counterparts.[19–21] Particularly, the atomic thickness of graphene lenses makes it possible to shrink the thickness of optical systems down to the sub nanometer scale, its planar nature provides the possibility of its integration with current planar optoelectronic systems and the propagation of optical signals as the highly confined SPP waves on the graphene sheets opens the way for realization of compact optical systems.[22] Besides that the complexity in design and difficulty in the fabrication process of noble metal based plasmonic lenses due to their small size, have been obviated in graphene ones. And at last, the operation and tunability of graphene lenses in the terahertz gap region of the electromagnet spectrum pave the way for accomplishment of the above mentioned new applications in these frequencies.

[a]Author to whom correspondence should be addressed. Electronic mail: Hadiseh_Nasari@ee.kntu.ac.ir.

In this paper, we introduce a perturbed ground plane design procedure leading to a specific conductivity profile along a strip on a background graphene layer, which effectively manipulates a guided SPP plane wave normally incident upon it. The effective mode index of propagating SPPs on the graphene sheet is taken into account to evaluate the physical principle of beam manipulation. We employ this technique to characterize beam focusing action. Furthermore, thanks to the tunability of graphene conductivity with applied gate voltage, focus tuning is investigated. Certainly, it can be extended to achieve other graphene based long needed functional terahertz components such as splitters, deflectors and so on. In fact, the noticeable electrical tunability of the propagating terahertz SPP wave with low loss and high confinement on graphene, the capability of high level integration and compatibility with silicon based integrated circuits besides the straightforward design and simple fabrication process nominate the proposed graphene based lens as a more appropriate candidate in comparison with its metamaterial,[23] photonic crystal,[24] dielectric and noble metal based plasmonic counterpart for highly demanded tunable terahertz lenses in the industry.

II. ON THE TUNABLE OPTICAL CONDUCTIVITY OF GRAPHENE

The anisotropic complex surface conductivity of graphene, a fundamental parameter to describe its optical and electronic properties in the terahertz, infrared and visible regions, according to (1), is strongly dependent on the radian frequency ω, the chemical potential μ_c (controlled by an electrostatic bias field E_0 or modifying the initial doping), a phenomenological scattering rate Γ, the temperature T, and an applied magneto static bias field B_0[25]

$$\bar{\bar{\sigma}}(\omega, \mu_c(E_0), \Gamma, T, B_0) = \hat{x}\hat{x}\sigma_{xx} + \hat{x}\hat{z}\sigma_{xz} + \hat{z}\hat{x}\sigma_{zx} + \hat{z}\hat{z}\sigma_{zz}. \quad (1)$$

For the sake of simplicity and in the absence of magnetic field, this conductivity will be isotropic (i.e., $\sigma_{xz} = \sigma_{zx} = 0$) and can be modeled by the well–known Kubo formalism (assuming $\exp(j\omega t)$ time harmonic variation)[25]

$$\begin{aligned}\sigma_{xx} = \sigma_{zz} &= \sigma_d(\omega, \mu_c, \Gamma, T) \\ &= \frac{je^2}{\pi\hbar^2(\omega - j2\Gamma)} \int_0^\infty \varepsilon \left(\frac{\partial f_d(\varepsilon)}{\partial \varepsilon} - \frac{\partial f_d(-\varepsilon)}{\partial \varepsilon} \right) d\varepsilon \\ &\quad - \frac{je^2(\omega - j2\Gamma)}{\pi\hbar^2} \int_0^\infty \frac{f_d(-\varepsilon) - f_d(\varepsilon)}{(\omega - j2\Gamma)^2 - 4(\varepsilon/\hbar)^2} d\varepsilon, \end{aligned} \quad (2)$$

where $-e$ is the electron charge, $\hbar = h/2\pi$ is the reduced Planck's constant, $f_d(\varepsilon) = \{\exp[(\varepsilon - \mu_c)/K_BT] + 1\}^{-1}$ is the Fermi-Dirac distribution, and K_B is the Boltzmann's constant. While the first term in (2) is due to the intraband contribution, the second term is due to the interband contributions. After some straightforward calculations, these integrals can be simplified to[25]

$$\sigma_{intra}(\omega, \mu_c, \Gamma, T) = -\frac{je^2 K_B T}{\pi\hbar^2(\omega - j2\Gamma)} \times \left[\frac{\mu_c}{K_B T} + 2\, ln(\exp(-\mu_c/K_B T) + 1) \right], \quad (3)$$

$$\sigma_{inter}(\omega, \mu_c, \Gamma, T) = -\frac{je^2}{4\pi\hbar}\, ln\left[\frac{2|\mu_c| - (\omega - j2\Gamma)\hbar}{2|\mu_c| + (\omega - j2\Gamma)\hbar} \right]. \quad (4)$$

It is worthy of note that the assumption of $|\mu_c|, \hbar\omega \gg K_BT$ is taken into account to simplify the calculation of interband conductivity. For all of the presented results, in this paper, $T = 300\,\mathrm{K}$ and $\Gamma = 0.41\,\mathrm{meV}$ are considered.

Figs. 1(a) and 1(b) show the variations of the real and imaginary parts of the graphene conductivity with frequency and chemical potential.

III. DESIGN PRINCIPLE AND NUMERICAL TECHNIQUE

The influence of applied voltage between the graphene sheet and the substrate is incorporated into the graphene conductivity via chemical potential and Fermi-Dirac distribution. By considering the relation (5) between the extra

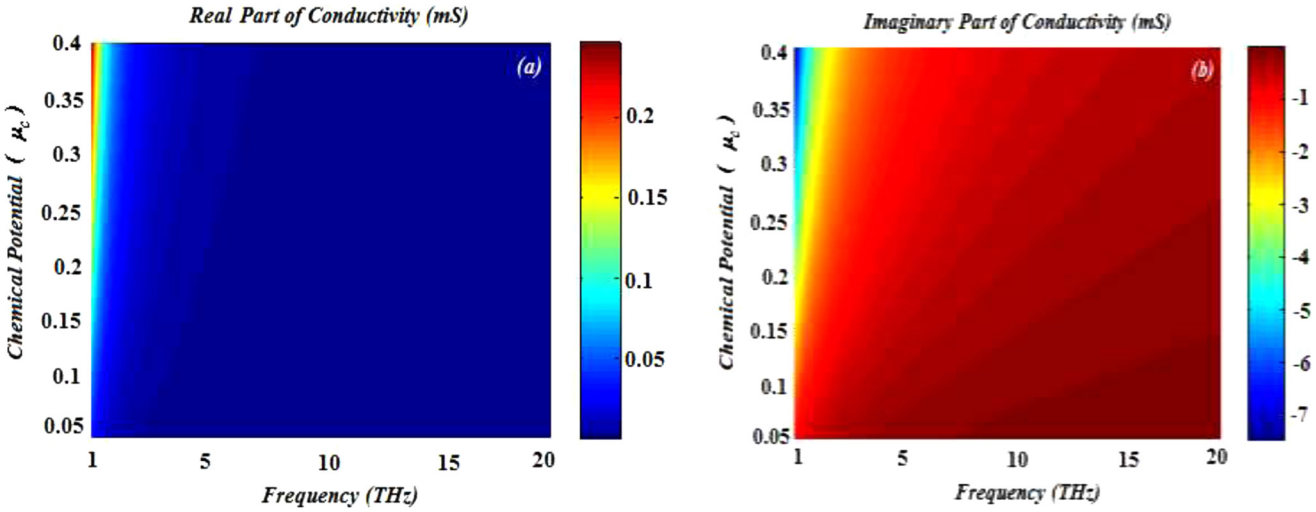

FIG. 1. The variation of the (a) real and (b) imaginary parts of the conductivity of 1 nm thick graphene layer.

charge carrier density and the applied voltage in an isolated graphene sheet[25]

$$n_s = V_g \varepsilon_0 \varepsilon_r / ed. \tag{5}$$

The chemical potential can be calculated via[25,26]

$$n_s = 2/\pi\hbar^2 v_F^2 \int_0^\infty \varepsilon(f_d(\varepsilon) - f_d(\varepsilon + 2\mu_c))d\varepsilon, \tag{6}$$

where $-e$ is the electron charge, d is the intermediate layer (the layer between silicon substrate and graphene) thickness, ε_0 and ε_r are the permittivity and the relative permittivity of the air and the intermediate layer, respectively, and V_g is the applied voltage. From the practical point of view, we should mention that the silicon substrate with a proper level of doping can act as a gate electrode and the voltage can be applied between the substrate and a gold or silver electrode on the graphene layer.

The variation of the required applied voltage by chemical potential and the intermediate layer thickness as well as chemical potential and the intermediate layer relative permittivity are shown plotted in Figs. 2(a) and 2(b), respectively. The variation of silicon dioxide thickness by the applied voltage and chemical potential is also depicted in Fig. 2(c).

By defining very small thickness of Δ for graphene, the volume conductivity of graphene will be $\sigma_{g,v} \equiv \sigma_g/\Delta$; thus, the volume current density is $\boldsymbol{J} = \sigma_{g,v}\boldsymbol{E}$. Considering the Maxwell equation of $\nabla \times \boldsymbol{H} = \boldsymbol{J} + j\omega\varepsilon_0\boldsymbol{E} = (\sigma_{g,v} + j\omega\varepsilon_0)\boldsymbol{E}$, the equivalent complex permittivity of Δ thick graphene layer is obtained $\varepsilon_{g,eq} \equiv \varepsilon_0 + \sigma_{g,i}/\omega\Delta - j\sigma_{g,r}/\omega\Delta$. Where $\sigma_{g,r}$ and $\sigma_{g,i}$ imply to the real and imaginary parts of the graphene conductivity. So for very small thickness of Δ, the real and imaginary parts of the equivalent permittivity are $Re(\varepsilon_{g,eq}) = \varepsilon_0 + \sigma_{g,i}/\omega\Delta \approx \sigma_{g,i}/\omega\Delta$ and $Im(\varepsilon_{g,eq}) \approx -\sigma_{g,r}/\omega\Delta$, respectively. This shows that the real part of graphene permittivity can be positive or negative.[27]

In the case of $\sigma_{g,i} < 0$ and hence $Re(\varepsilon_{g,eq}) < 0$, a characteristic, which is seen in the noble metals in the near infrared frequencies, a TM SPP wave will be supported by graphene layer, while in the case of $\sigma_{g,i} > 0$, a weakly guided TE SPP wave might be present.

It is shown that the dispersion relation for a material with complex permittivity of ε_m and thickness of Δ, surrounded by free space, which supports odd TM SPP is[28]

$$\coth\left(\sqrt{\beta^2 - \omega^2\mu_0\varepsilon_m}\,\Delta/2\right) = -\frac{\varepsilon_m}{\varepsilon_0}\frac{\sqrt{\beta^2 - \omega^2\mu_0\varepsilon_0}}{\sqrt{\beta^2 - \omega^2\mu_0\varepsilon_m}}. \tag{7}$$

By substituting ε_m with the complex permittivity of graphene, denoted above, and letting $\Delta \to 0$ the dispersion relation of the TM SPP optical wave along a graphene layer can be expressed as[29]

$$\beta_{spp} = k_0\sqrt{1 - \left(\frac{2}{\sigma_g\eta_0}\right)^2}, \tag{8}$$

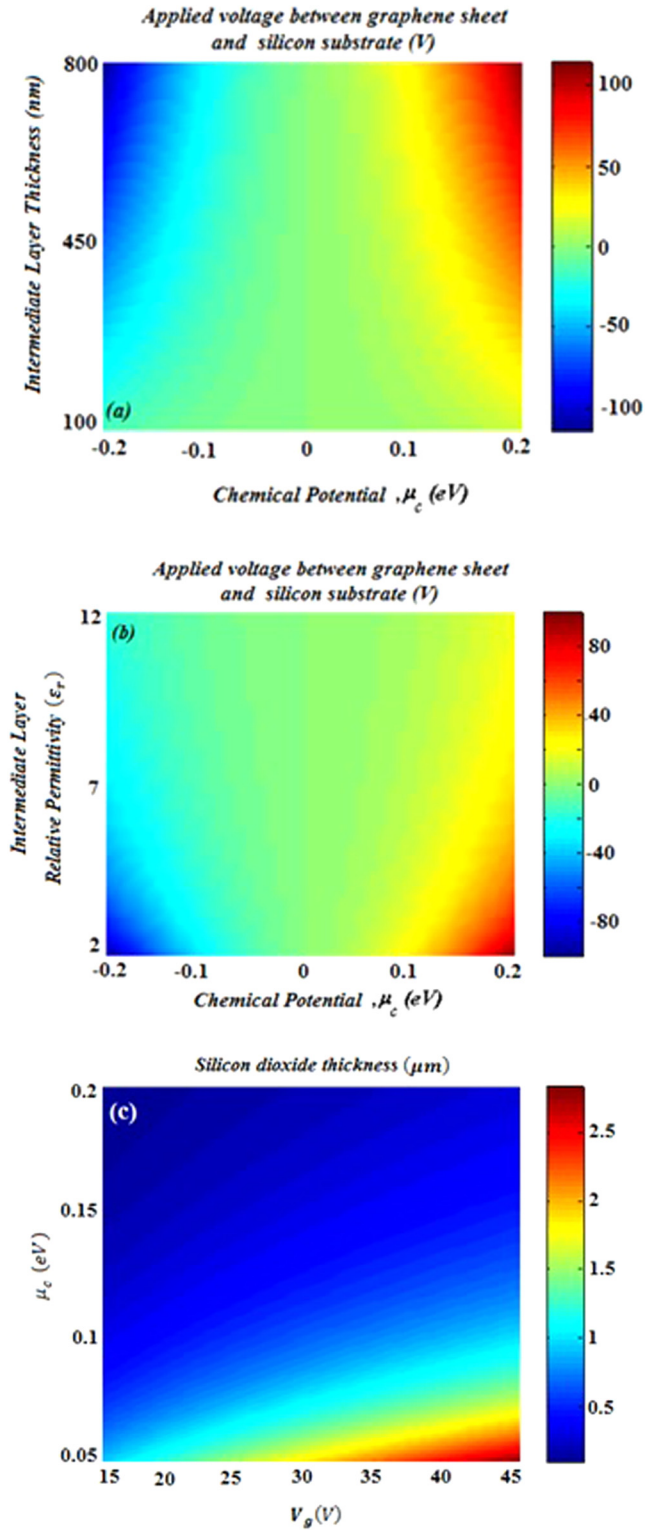

FIG. 2. The variation of applied voltage in volt between the graphene sheet and the silicon substrate with (a) chemical potential and the intermediate layer thickness. The intermediate layer relative permittivity is taken 3.9 (b) chemical potential and the intermediate layer permittivity. The intermediate layer thickness is taken 400 nm and (c) the variation of silicon dioxide intermediate layer thickness by the applied voltage and chemical potential.

where η_0 and k_0 are the intrinsic impedance of free space and the free space wave number, respectively.

As can be seen in the presented results of Fig. 1, the real part of graphene conductivity is much smaller than its

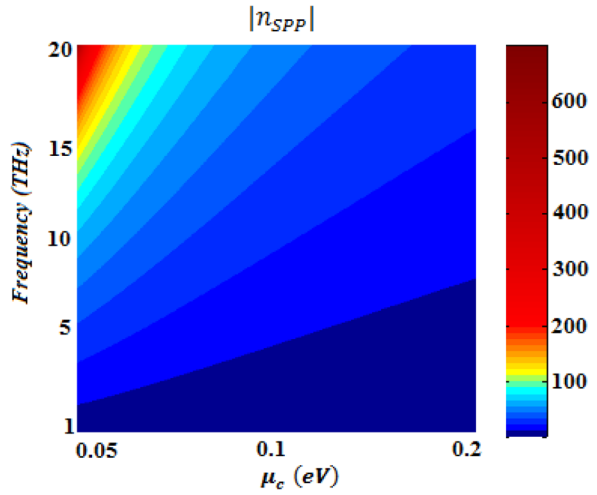

FIG. 3. The variation of the effective mode index of SPP with chemical potential and frequency.

imaginary part, so the dispersion relation can be approximated as[30]

$$n_{spp} = \beta_{spp}/k_0 \approx 2/\sigma_{g,i}\,\eta_0. \tag{9}$$

The variation of n_{spp}, the effective mode index of SPP, with chemical potential and frequency is shown plotted in Fig. 3.

As it is shown in Refs. 19 and 31 and is widely known, the plane wave normally incident upon a strip, bends toward the region of the strip with higher effective mode index of SPP, which provides more phase retardation for the light passing through its width. According to Fig. 3, this can be achieved by producing lower chemical potential. For this purpose, according to Fig. 2(c), the thickness of silicon dioxide intermediate layer at a constant applied voltage should increase. Fig. 4(a) schematically shows our proposed graphene based lens on this basis. Its cross section is also depicted in Fig. 4(b). By decreasing the silicon dioxide layer thickness from center to the side of the strip, the chemical potential increases and the effective mode index of SPP decreases. By this way, the phase retardation of transmitted light through the width of the strip will decrease from its center to the side, which is the required condition for beam focusing action.

In what follows, we profit from FDTD numerical technique to simulate the characteristics of SPP wave propagation. The lateral dimensions of graphene layer in our proposed lens are chosen in the order of 100 micrometer, which is much larger than its 1 nm thickness, so it seems reasonable that in order to avoid high discretization density inside the graphene sheet, which certainly requires large amounts of computer memory and computation time besides nearly no effect on the final result, as far as it is extremely small compared to the wavelength, the simulation to be conducted via 2D FDTD. The outer boundary of the computation lattice is terminated to the convolutional perfectly matched layer (CPML) to dissipate the outgoing waves. The grid sizes are chosen $\Delta x = \Delta z = 0.5\,\mu$m and the time step is set $\Delta t = 0.95/(c\sqrt{(\Delta x)^{-2} + (\Delta z)^{-2}})$, which is achieved by Courant stability condition, where c is the speed of light in the free space.[32]

Considering (3) and (4), it is found that in the far-infrared regime, the contribution of interband electron transition in the graphene conductivity is negligible and should be taken into account at higher frequencies depending on the chemical potential.[33] So in modeling the dispersive behavior of graphene at 15 THz only the intraband term is incorporated and the relevant current is calculated via[34]

$$\sigma_{gr} = -jA/(B\omega - jZ)\,, \tag{10}$$

$$A = e^2 K_B T(\mu_c/K_B T + 2ln(\exp(-\mu_c/K_B T) + 1))/\Delta, \tag{11}$$

$$B = \pi\hbar^2, \tag{12}$$

$$Z = 2\pi\hbar^2\Gamma, \tag{13}$$

$$\dot{\boldsymbol{J}} = \sigma_{gr}\dot{\boldsymbol{E}}, \tag{14}$$

where dot denotes the frequency domain; then, the conductivity current in the time domain will be[34]

$$J_x|_{i,k}^{n+3/2} = \frac{2B - Z\Delta t}{2B + Z\Delta t} J_x|_{i,k}^{n+1/2} + \frac{2A\,\Delta t}{2B + Z\Delta t} E_x|_{i,k}^{n+1} \tag{15}$$

with equivalent equation holding for J_z.

To validate our FDTD code in its full three dimensional case, the transmission, reflection, and absorption spectra for a normally incident plane wave upon infinite graphene sheets, which is schematically shown in Fig. 5(a), are compared with analytical expression from transfer matrix method (TMM)[35] and the results are presented in Fig. 5(b). Infinite

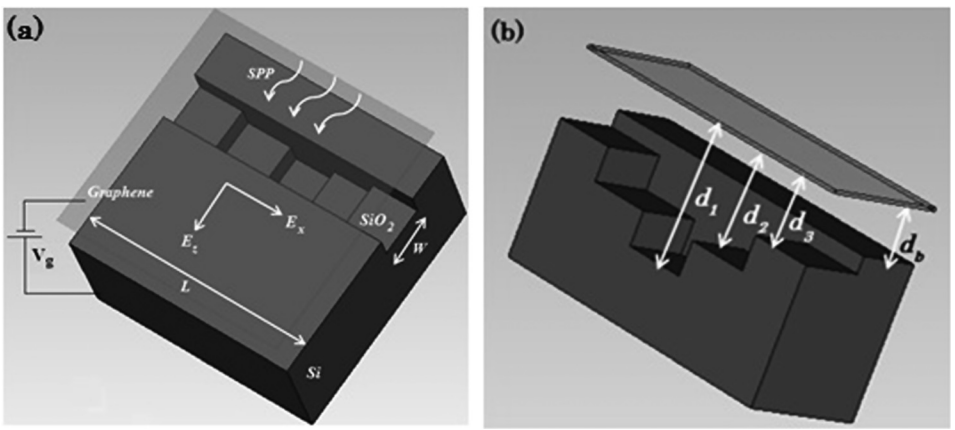

FIG. 4. (a) Schematic representation of proposed graphene based lens. (b) Cross section of the proposed lens in panel (a).

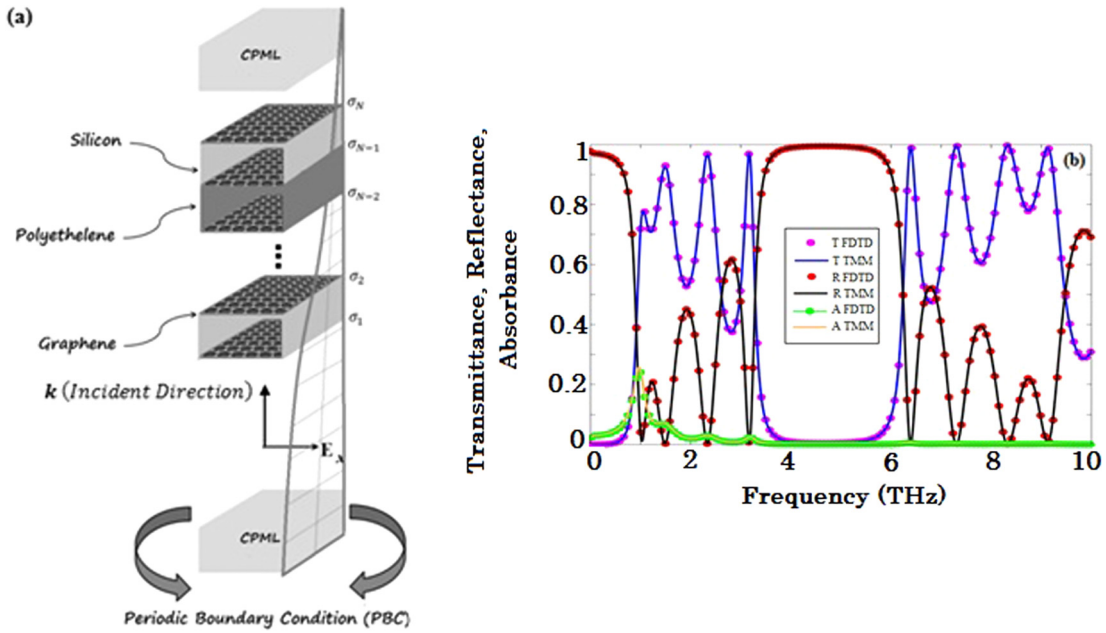

FIG. 5. (a) Schematic representation of multiple graphene-dielectric structure. (b) The Transmission (T), Reflection (R), and Absorption (A) spectra, which are computed by both TMM and FDTD for a graphene -dielectric multilayer structure. 8 dielectric layers are sandwiched between 9 graphene layers. The dielectric layers are polyethylene and silicon with 5 and 10 micrometer thickness and 2.25 and 11.9 dielectric constant, respectively. The chemical potential of the intermediated graphene layers is set to be 0.1 eV.

graphene sheets in the lateral sides are described by periodic boundary condition (PBC).

IV. SIMULATION RESULTS AND DISCUSSION

In the following presented simulation results, the width (W) and the length (L) of the strip are chosen 25 and 100 micrometer, respectively, which by currently developed techniques to pattern large scale graphene sheets are achievable.[16] The length of the strip is equally divided to five parts by 20 micrometer length. The thickness of silicon dioxide intermediate layer is chosen $d_1 = 800\,\text{nm}$, $d_2 = 600\,\text{nm}$, and $d_3 = 400\,\text{nm}$ from center to the side of the strip, respectively. The background graphene layer is formed on a 380 nm thickness silicon dioxide layer. The applied voltage between the graphene sheet and the substrate and the corresponding chemical potential of the graphene layer are tabulated in Table I. It is noteworthy that the dimensions of steps in silicon ground plane are selected such that with current etching techniques it would be straightforward to achieve. Thermal oxidation process can also be implemented to create silicon dioxide spacer.

TABLE I. Chemical potential variation of graphene at different silicon dioxide thicknesses by applied voltage between the graphene sheet and the substrate. The chemical potential of the background graphene layer is denoted by $\boldsymbol{\mu_{cb}}$. $\boldsymbol{\mu_{c1}}$, $\boldsymbol{\mu_{c2}}$, **and** $\boldsymbol{\mu_{c3}}$ imply to the chemical potential of the central to the side parts of the strip.

V_g (V)	μ_{c1} (eV)	μ_{c2} (eV)	μ_{c3} (eV)	μ_{cb} (eV)
15	0.0565	0.0688	0.089	0.092
20	0.069	0.083	0.106	0.109
25	0.0795	0.095	0.1205	0.124
30	0.0892	0.106	0.1335	0.1372
35	0.098	0.116	0.1455	0.1495
40	0.106	0.125	0.1563	0.1595
45	0.1135	0.1335	0.1665	0.1715

The time-average magnetic field intensity distributions for different values of V_g are shown in Figs. 6(a)–6(d) and clearly indicate the appearance of focal point in the result of designed chemical potential variation along the strip. Here, we recall that the large momentum mismatch between incoming free space electromagnetic wave and propagating plasmons on graphene sheet is a big challenge that makes the excitation of SPPs on graphene a difficult task. However, several mechanisms are reported to enable the coupling of incident free-space light to guided SPPs such as using Otto configuration composed of a bulk prism of high dielectric constant, enhancing the in plane momentum of incoming light by using the apex of an unilluminated nanotip and so on.[36,37]

These figures interestingly show that by increasing the applied voltage, the focal point has dropped to the closer distances to the lens. Focal length is measured as the distance between the output surface of the strip and the point with highest intensity on the x–axis of the lens. The magnetic field intensity on the lens axis along the x direction representing Focal Length (FL) and on the focal plane representing the full-width half-maximum (FWHM) are shown in Figs. 7(a) and 7(b), respectively.

To find out the origin of focus moving, we should recall that the focal length depends on the speed of light in the strip region compared to the background graphene layer. In fact, for larger difference of light speed, the focus drops to closer distance from the exit surface of the strip.[38] For this purpose, we have calculated n_{spp} for central brick (possessing the highest one) on the strip and background graphene layer at different values of applied voltage and the results are

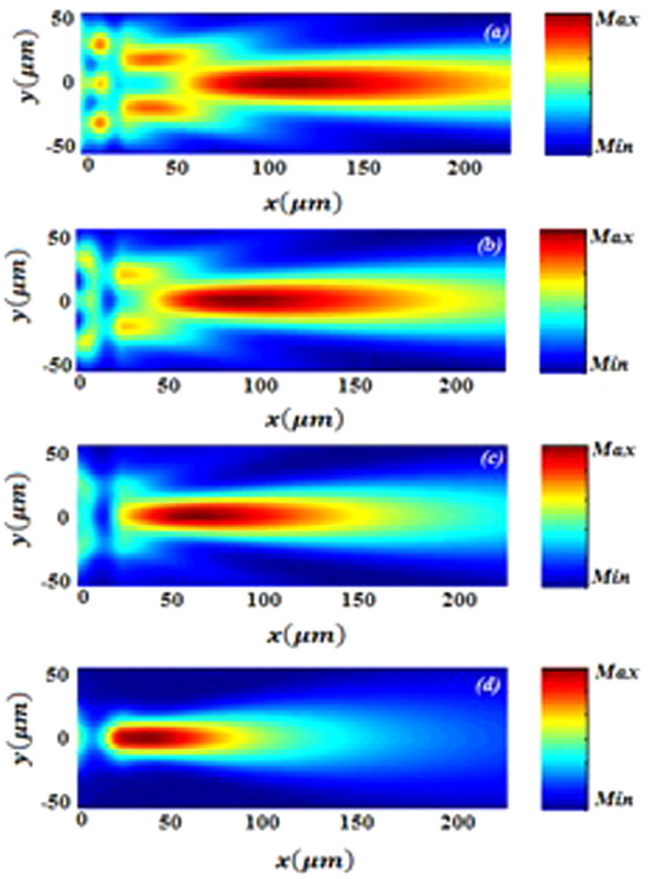

FIG. 6. Time-average magnetic field intensity distribution for (a) $V_g = 15$ V, (b) $V_g = 25$ V, (c) $V_g = 35$ V, and (d) $V_g = 45$ V.

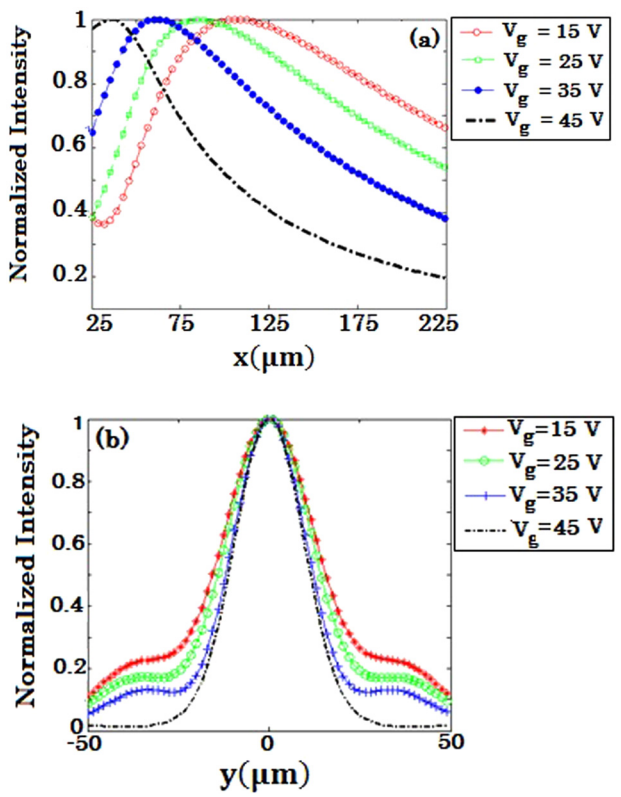

FIG. 7. (a) The magnetic field intensity on the lens axis along the x direction and (b) on the focal plane for the proposed lens in Fig. 4.

TABLE II. Comparison of effective mode index for different gate voltages.

Gate voltage (V)	$n_{spp,1}$	$n_{spp,b}$	$1/n_{spp,b} - 1/n_{spp,1}$
15	99.3	51.5	0.0093
25	61.6	36.5	0.0111
35	47.8	29.7	0.0127
45	40.35	25.6	0.0142

reported in Table II. The light speed difference is proportional to $1/n_{spp,b} - 1/n_{spp,1}$ and our calculations show that it increases by increasing the gate voltage. On this basis, inward focus movement upon increasing the applied gate voltage will be expected, which is in agreement with our presented FDTD simulations results above.

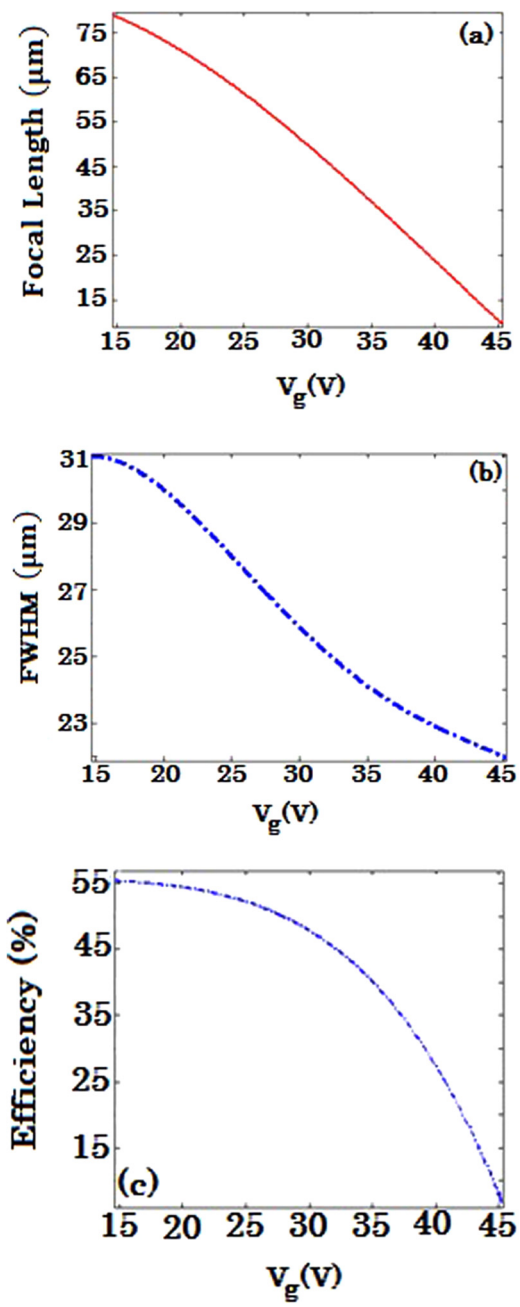

FIG. 8. The variation of (a) focal length (b) full-width half-maximum and (c) focusing efficiency with the applied voltage for the proposed lens in Fig. 4.

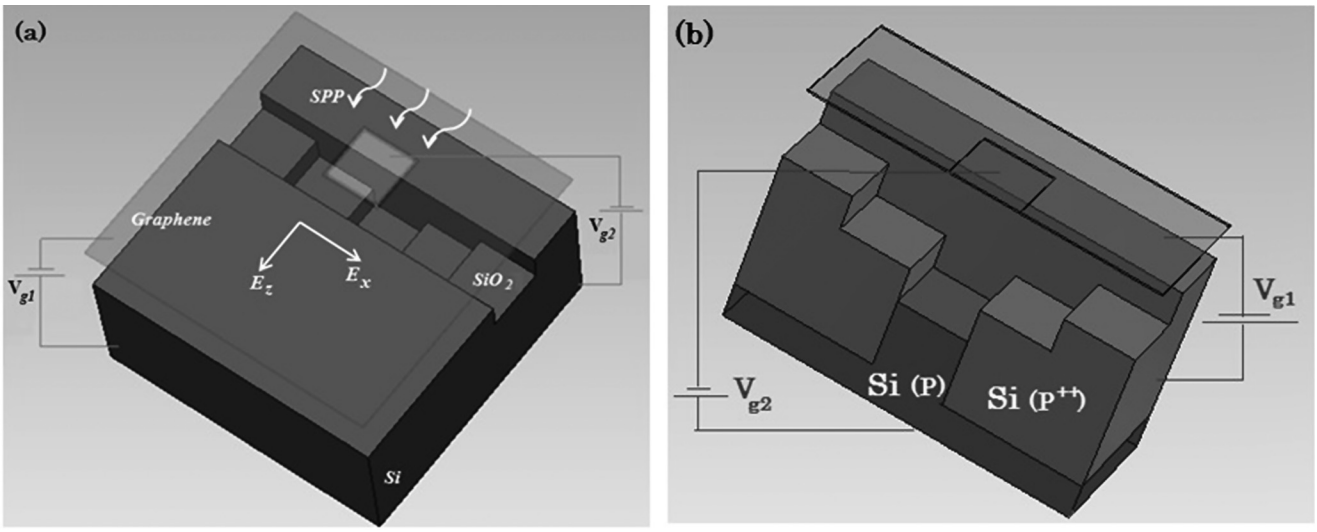

FIG. 9. (a) Schematic configuration of proposed graphene based lens to examine the effect of chemical potential change rate along the strip, (b) the cross section of proposed lens in panel (a).

The variation of FL and FWHM with the applied voltage between the graphene sheet and the substrate is depicted in Figs. 8(a) and 8(b), respectively. These results clearly illustrate that by increasing V_g both of the FL and FWHM decrease. The variation of efficiency of focusing by V_g, which is obtained by dividing the intensity of the focal point to the incident intensity, is also plotted in Fig. 8(c). It is worthy of note that according to Fig. 7(b), the side lobe level is also dropped considerably by increase in the gate voltage.

The rate of change in the effective mode index along the strip can also affect the focusing properties of the lens. To explore this phenomenon, the shown plotted configuration in Fig. 9(a) is proposed. It is worthy to note that, in this case, the graphene sheet remains continuous and a discrete gating structure is employed. Indeed, different levels of doping for silicon substrate beneath the shown opaque region in Fig. 9(a) are created as it is clearly rendered in its cross section in Fig. 9(b). The regions in the substrate with different levels of doping can be easily created by ion implantation technique.

By decreasing V_{g2}, while V_{g1} is kept constant, μ_{c1}, the chemical potential of the central part of the strip, decreases and according to Fig. 3 n_{spp} increases, so by the raise in the n_{spp} and hence the total phase difference between the central and side parts of the strip, a reduction in the focal length will be resulted as it is illustrated by the magnetic field intensity along the x direction in Fig. 10.

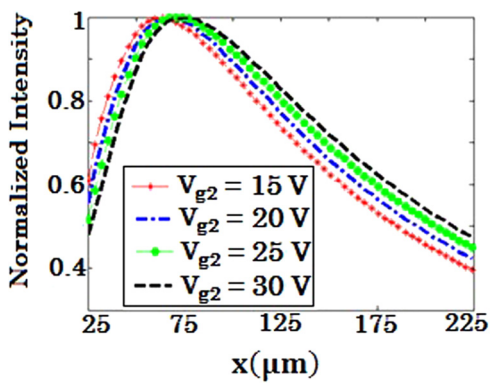

FIG. 10. The magnetic field intensity along the x direction of the lens for different values of applied voltages to the cental part on the graphene strip, while $\mathbf{V_{g1} = 30\,V}$.

To more clearly demonstrate this phenomenon, consider the phase of transmitted light through the width of the strip, for the case of normal incident light, expressed by[39]

$$\Delta\varphi \approx \Delta\phi_1 + \Delta\phi_2 + Re(\beta_{spp}) \cdot W - \theta, \qquad (16)$$

where $\Delta\phi_1$ and $\Delta\phi_2$ are accompanied phase changes at the entrance and exit surfaces, which cancel each other when the illuminated and unilluminated sides are the same, $Re(\beta_{spp}) \cdot W$ is the phase retardation of SPPs propagating in the width of the strip and θ originates from multiple reflections between the entrance and exit surfaces, but $Re(\beta_{spp}) \cdot W$ plays dominant role in calculating the phase of transmitted light. W is the thickness of the strip and β_{spp} can be calculated from (8).

According to (16), the total phase difference at the output surface of the strip are calculated $0.18\,\pi$, $0.21\,\pi$, $0.24\,\pi$, and $0.42\,\pi$ for V_{g2} equal to 30 V, 25 V, 20 V, and 15 V, respectively.

The variation of FL and FWHM is also presented in Figs. 11(a) and 11(b), respectively.

Finally, it should be mentioned that since it is practically impossible to create a continuous variation of effective mode index of propagating SPPs along the strip, we have divided the strip to five discrete bricks with certain values of conductivity, which is accomplished by applying gate voltage on an uneven ground plane. Certainly, increasing the number of bricks and optimization of the geometrical properties of each brick should lead to improved performance of the proposed devices.

Furthermore, for the sake of numerical simulation simplicity, piece wise constant conductivity assumption in this inhomogeneous biasing scheme is employed, i.e., hard boundary condition is taken into account, which gives a basic insight of the device performance. Certainly, the precise conductivity profile determination will be achieved by exact solution of Laplace's equation.[40]

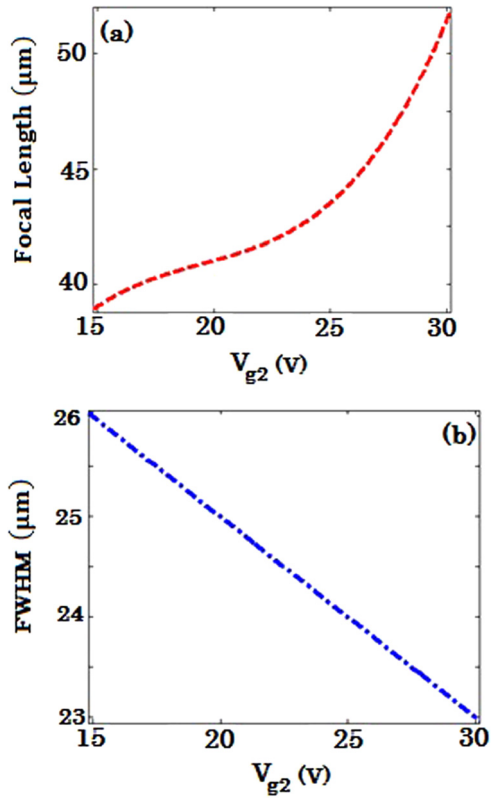

FIG. 11. The variation of (a) focal length and (b) full-width half-maximum with different applied voltages to the cental part on the graphene strip, while $\mathbf{V_{g1} = 30\,V}$.

V. CONCLUDING REMARKS

To conclude, we have presented a tunable graded index graphene based planar lens. On the basis of the effective mode index of propagating SPPs on the graphene sheet, a ground plane design procedure has been introduced, which leads to the formation of a specific conductivity profile along a strip with the capability of effective manipulation of a guided SPP plane wave normally incident upon it. By taking advantage of the graphene chemical potential electrostatic tunability, the possibility of focal length modulation via external applied gate voltage between the graphene sheet and the substrate has been investigated theoretically and simulated numerically via FDTD technique. The introduced design procedure, in this paper, can also be employed to achieve beam splitting and deflecting phenomena. The proposed active manipulation of terahertz beam on the one atom thick graphene platform opens interesting opportunities on signal processing, scan imaging, and so on.

[1]C. Rizza, A. Ciattoni, E. Spinozzi, and L. Columbo, Opt. Lett. **37**, 3345 (2012).
[2]K. S. Novoselov, A. K. Geim, S. V. Morozov, D. Jiang, Y. Zhang, S. V. Dubonos, I. V. Grigorieva, and A. A. Firsov, Science **306**,666 (2004).
[3]K. S. Novoselov, A. K. Geim, S. V. Morozov, D. Jiang, M. I. Katsnelson, I. V. Grigorieva, S. V. Dubonos, and A. A. Firsov, Nature **438**, 197 (2005).
[4]A. K. Geim and K. S. Novoselov, Nature Mater. **6**, 183(2007).
[5]P. Weis, J. L. Garcia-Pomer, M. Hoh, B. Reinhard, A. Brodyanski, and M. Rahm, ACS Nano **6**, 9118 (2012).
[6]P. Y. Chen and A. Alu, ACS Nano **5**, 5855 (2011).
[7]F. Xia, T. Mueller, Y. Lin, A. V. Garcia, and P. Avouris, Nature Nano Tech. **4**, 839 (2009).
[8]M. Liu., X. Yin, E. Avila, B. Geng, T. Zentgraf, L. Ju, F. Wang, and X. Zhang, Nature **474**, 64 (2011).
[9]J. S. Gomez-Diaz and J. P. Carrier, Opt. Express **21**, 15490 (2013).
[10]S. F. Busch, S. Schumann, C. Jansen, and M. Koch, Appl. Phys. Lett. **100**, 261109 (2012).
[11]S. Pisana, P. M. Braganca, E. E. Marinero, and B. A. Gurney, IEEE Trans. Magn. **46**, 1910 (2010).
[12]Y. V. Bludov, M. I. Vasilevskiy, and N. M. R. Peres, J. Appl. Phys. **112**, 084320 (2012).
[13]F. H. L. Koppens, D. E. Chang, and F. Abajo, Nano Lett. **11**, 3370 (2011).
[14]S. Stankovich, D. A. Dikin, R. D. Piner, K. A. Kohlhaas, A. Kleinhammes, Y. Jia, Y. Wu, S. T. Nguyen, and R. S. Ruoff, Carbon **45**, 1558 (2007).
[15]C. Berger, Z. Song, X. Li, X. Wu, N. Brown, C. Naud, D. Mayou, T. Li, J. Hass, A. N. Marchnkov, E. H. Conrad, P. N. First, and W. A. D. Heer, Science **312**, 1191 (2006).
[16]K. S. Kim, Y. Zha, H. Jang, S. Y. Lee, J. M. Kim, K. S. Kim, J. S. Ahn, P. Kim, J. Y. Choi, and B. H. Hong, Nature Lett. **457**, 706 (2009).
[17]A. C. Ferrari, J. C. Meyer, V. C. Scardaci, C. Casiraghi, M. Lazzeri, F. Mauri, F. Piscanec, D. Jiang, K. S. Novoselov, S. Roth, and A. K. Geim, Phys. Rev. Lett. **97**, 187401 (2006).
[18]P. N. Incze, Z. Osvath, K. Kamars, and L. P. Biro, Carbon **46**, 1435 (2008).
[19]L. Verslegers, P. B. Catrysse, Z. Yu, J. S. White, E. S. Barnard, M. L. Brongersma, and S. Fan, Nano Lett. **9**, 235 (2009).
[20]H. Nasari and M. S. Abrishamian, Plasmonics **8**, 1675 (2013).
[21]H. Shi, C. Wang, C. Du, X. Luo, X. Dong, and H. Gao, Opt. Express **13**, 6815 (2005).
[22]A. Vakil and N. Engheta, Phys. Rev. B **85**, 075434 (2012).
[23]J. Neu, B. Krolla, O. Paul, B. Reinhard, R. Beigang, and M. Rahm, Opt. Express **18**, 27748 (2010).
[24]A. Martinez, H. Miguez, A. Griol, and J. Marti, Phys. Rev. B **69**, 165119 (2004).
[25]G. W. Hanson, IEEE Trans. Antennas Propag. **56**, 747 (2008).
[26]V. Ryzhii, A. Satou, and T. Otsouji, J. Appl. Phys. **101**, 024509 (2007).
[27]A. Vakil and N. Engheta, Science **332**, 1291 (2011).
[28]A. Alu and N. Engheta, J. Opt. Soc. Am. B **23**, 571 (2006).
[29]G. W. Hanson, Appl. Phys. **103**, 064302 (2008).
[30]H. J. Xu, W. B. Lu, Y. Jiang, and Z. G. Dong, Appl. Phys. Lett. **100**, 051903 (2012).
[31]Z. Sun and H. K. Kim, Appl. Phys. Lett. **85**, 642 (2004).
[32]A. Toflaove and S. C. Hagness, *Computational Electrodynamics: The Finite-Difference Time- Domain Method* (Artech House, Boston, USA, 2005).
[33]V. Nayyeri, M. Soleimani, and O. M. Ramahi, IEEE Trans. Antennas Propag. **61**, 6107 (2013).
[34]G. D. Bouzinas, N. V. Kantartzis, C. S. Antonopoulos, and T. D. Tsiboukis, IEEE Trans. Magn. **48**, 379 (2012).
[35]T. Zhan, X. Shi, Y. Dai, X. Liu, and J. Zi, J. Phys. Condens. Matter **25**, 215301 (2013).
[36]J. S. G. Diaz, M. E. Morote, and J. P. Carrier, Opt. Express **21**, 24856 (2013).
[37]Y. V. Bludov, A. Ferreira, N. M. R. Peres, and M. I. Vasilevskiy, Int. J. Mod. Phys. B **27**, 1341001 (2013).
[38]B. A. E. Saleh and M. C. Teich, *Fundamental of Photonics* (John Wiley & Sons, Hoboken, New Jersey, USA, 2007).
[39]M. Born and E. Wolf, *Principles of Optics* (Pergamon Press, New York, USA, 1975).
[40]E. Forati and G. W. Hanson, J. Opt. **15**, 114006 (2013).